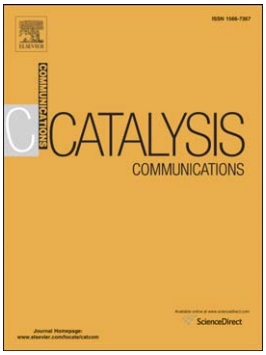

Visible Light Induced Decomposition of Organic Compounds on WO_3 Loaded PtPb Co-catalysts

Takao Gunji, Takashi Tsuda, Arockiam John Jeevagan, Masanari Hashimoto, Toyokazu Tanabe, Shingo Kaneko, Masahiro Miyauchi, Govindachetty Saravanan, Hideki Abe, Futoshi Matsumoto

PII: S1566-7367(14)00275-1
DOI: doi: 10.1016/j.catcom.2014.07.013
Reference: CATCOM 3970

To appear in: *Catalysis Communications*

Received date: 30 May 2014
Revised date: 4 July 2014
Accepted date: 5 July 2014

Please cite this article as: Takao Gunji, Takashi Tsuda, Arockiam John Jeevagan, Masanari Hashimoto, Toyokazu Tanabe, Shingo Kaneko, Masahiro Miyauchi, Govindachetty Saravanan, Hideki Abe, Futoshi Matsumoto, Visible Light Induced Decomposition of Organic Compounds on WO_3 Loaded PtPb Co-catalysts, *Catalysis Communications* (2014), doi: 10.1016/j.catcom.2014.07.013

Visible Light Induced Decomposition of Organic Compounds on WO_3 Loaded PtPb Co-catalysts

Takao Gunji, [a] Takashi Tsuda,[a] Arockiam John Jeevagan, [a] Masanari Hashimoto, [a] Toyokazu Tanabe, [a] Shingo Kaneko,[a] Masahiro Miyauchi,[b,c] Govindachetty Saravanan,[d] Hideki Abe,[c,e] Futoshi Matsumoto* [a]

[a]Department of Material and Life Chemistry, Kanagawa University, 3-27-1, Rokkakubashi, Kanagawa-ku, Yokohama, Kanagawa 221-8686, Japan.

[b]Department of Metallurgy and Ceramic Science, Graduate School of Science and Engineering, Tokyo Institute of Technology, 2-12-1 Ookayama, Meguro-ku, Tokyo, 152-8552, Japan

[c]PRESTO, Japan Science and Technology Agency (JST), 4-1-8 Honcho, Kawaguchi, Saitama 332-0012, Japan.

[d]CSIR-National Environmental Engineering Research Institute (CSIR-NEERI) Nehru Marg, Nagpur 440020, India.

[e]National Institute for Materials Science (NIMS), Sengen 1-2-1 Sengen, Tsukuba, Ibaraki 305-0047, Japan

Abstract

Tungsten oxide (WO_3)-supported ordered intermetallic PtPb nanoparticles (PtPb NPs/WO_3) were prepared through a co-reduction of Pt and Pb precursors with sodium borohydride in anhydrous methanol containing WO_3. The PtPb NPs/WO_3 were characterized based on the crystal structure obtained through powder X-ray diffraction (*p*XRD) as well as X-ray photoemission spectroscopy (XPS) and transmission electron microscopy (TEM). The formation of an ordered PtPb intermetallic phase on the WO_3 surface was confirmed. The PtPb NPs/WO_3 were more efficient when decomposing acetic acid (AcOH) and acetaldehyde (AcH) with visible light irradiation compared to the same process over WO_3 loaded with Pt nanoparticles (Pt NPs/WO_3).

Keywords

Photocatalysis, Co-catalyst, Ordered Intermetallic Compound, Photo-decomposition.

Highlights

- The WO_3 supported PtPb catalysts was synthesized.
- The formation of PtPb catalysts were characterized with TEM and XPS.
- The photocatalytic activities of the PtPb/WO_3 were investigated.

Introduction

Semiconductor photocatalysts, such as titanium oxide (TiO_2) and tungsten oxide (WO_3), have received significant attention for several decades because they are a potential solution for the current energy and environmental problems. Semiconductor photocatalysts are versatile candidates for environment remediation [1], water splitting [2], CO_2 reduction [3] and solar energy conversion [4]. Recently, numerous visible light-driven semiconductor photocatalysts have been developed [5]. Metal oxides, particularly WO_3, have attracted attention because they act as ideal visible light photocatalysts; this behavior is attributed due to their small band gap energies (2.4-2.8 eV) and the high oxidation power of their valence band holes [6]. However, WO_3 exhibits a low photocatalytic activity due to the rapid recombination of its photoexcited electrons and holes. To suppress this process and significantly increase the photocatalytic efficiency, the consumption of photoexcited electrons and holes should be enhanced using co-catalysts. Abe and co-workers have demonstrated that Pt-loaded WO_3 samples were highly efficient during the decomposition of organic compounds under visible light irradiation with an oxygen reduction, which consumed the photoexcited electrons [7]. Consequently, Pt nanoparticles (NPs) were used as co-catalysts with WO_3 to facilitate a multi-electron reduction of O_2, allowing O_2 to accept electrons despite the insufficient reduction potential of the conduction band electrons (in WO_3) during its single-electron reduction; furthermore, photocatalytic activity can be improved by selecting appropriate co-catalysts. Recently, a new approach that prevents the inherent problems of disordered alloy catalysts has been proposed by Abruña *et al*. toward highly active electrocatalysts for fuel cell applications [8]. In contrast with disordered alloys, intermetallic compounds with definite compositions and structures, such as PtPb and PtBi, exhibit excellent electrocatalytic performances toward FA oxidations in acidic solutions in

terms of their onset potentials and current densities [9, 10]. After the report by Abruña, many papers describing intermetallic NPs, such as PtBi, PtPb, Pt_3Ti and carbon black (CB)-supported intermetallic NPs, have been published for FA, MeOH and EtOH oxidations and oxygen reduction reactions (ORR) [11-13]. In our previous study, the electrocatalytic activity of the ordered intermetallic PtPb compounds exhibited higher electrocatalytic activity toward formic acid, methanol (MeOH) and ethanol (EtOH) oxidation [14] compared to conventional Pt-based alloys and Pt. In addition, we have recently reported that ordered PtPb intermetallic NPs accelerated oxygen reduction reactions (ORR) in acidic solutions [15]. Therefore, the ordered PtPb ordered intermetallic NPs should be competent co-catalysts at the oxidation and reduction sites on WO_3. We report a simple one-pot approach toward WO_3-supported ordered intermetallic PtPb NP catalysts. Furthermore, we investigated the effects of using ordered intermetallic PtPb compounds as co-catalysts with photocatalytic activity during the oxidative decomposition of acetic acid (AcOH) and acetaldehyde (AcH).

Experimental

The WO_3 particles were purchased from Kojundo Chemical Laboratory Co. Ltd. (Type: WWO04PB). Fine particulate WO_3 particles (50–200 nm) were separated from the commercial WO_3 powder, as reported in Ref. **7**. The photodeposited Pt NPs/WO_3 sample was synthesized as reported by Abe *et al.* [7]. The procedure used to prepare Pt NPs/WO_3 via chemical deposition with a Pt precursor and a reducing agent is described in the ESI†. The synthesis of PtPb NPs/WO_3 (PtPb loading: 1.0 wt%) proceeded as follows. WO_3 powder (0.5 g) was suspended in 15 mL of anhydrous methanol for 15 min in a two neck round bottomed flask. Afterwards, 0.013 mmole of chloroplatinic acid ($H_2PtCl_6{\cdot}6H_2O$, Wako, Japan) and 0.026 mmole of lead**(**II**)** acetate ($Pb(CH_3COO)_2$, Sigma-Aldrich) were dissolved in 15 mL of anhydrous methanol in a shielded vial under

Ar before being transferred to the WO_3 suspensions. The solution was stirred for 30 min to yield a homogeneous yellow solution. Afterwards, 3 mmole of sodium borohydride ($NaBH_4$, Sigma-Aldrich) in methanol was injected into the suspension to reduce the precursors. The product was centrifuged and washed with anhydrous methanol three times before being dried under vacuum. The as-prepared PtPb NPs/WO_3 were yellowish green. The other experimental conditions are described in the Supplementary Information.

Results and discussion

Fig. 1A shows the powder X-ray diffraction (*p*XRD) profiles of the WO_3, Pt NPs/WO_3 and PtPb NPs/WO_3 (Supplement information for the *p*XRD procedure). To confirm the formation of the ordered PtPb intermetallic NPs on the WO_3 through *p*XRD, the Pt loading on WO_3 was adjusted to 5 wt% on both the Pt NPs/WO_3 and PtPb NPs/WO_3, while 0.1 or 1.0 wt% Pt and ordered intermetallic PtPb were used when testing the photocatalytic activity. The simulated *p*XRD patterns for the Pt phase (face-centered cubic (fcc), *Fm*-3*m*, a = 0.3925 nm, JCPDS 04-0802) and the ordered intermetallic PtPb phase (NiAs structure, $P6_3/mmc$, $a = b$ = 0.426 nm, c = 0.548 nm) are denoted by the solid bars below the graph. The *p*XRD profile (Fig. 1A-(a)) for WO_3 shows several major peaks, which are attributed to monoclinic WO_3 (JCPDS 43-1035) In addition, the *p*XRD profiles (Fig. 1A-(b, c)) for the Pt NPs/WO_3 and the as-prepared PtPb NPs/WO_3 exhibit small characteristic peaks at 39.8° for Pt and at 41.0° and 42.4° for the ordered intermetallic PtPb phases. The retention of the *p*XRD peaks at 41.0 and 42.4°, even after heat-treating the as-prepared PtPb NPs/WO_3 (the reason for the heat-treatment will be explained in Fig. 3), could be ascribed to the formation of stable, ordered PtPb intermetallic NPs on the WO_3 (Fig. S1).

Figures 1 (B) and (C) show low- and high-resolution (HR)-TEM images of the annealed 1.0 wt% PtPb NPs/WO_3. Several low-resolution images were obtained from a PtPb NPs/WO_3 sample, as shown in Fig. S2, to show the particle size and the degree of dispersion of the PtPb NPs on the WO_3. The size distributions of the PtPb NPs were evaluated based on the sizes of approximately 100 particles in the TEM images. The average diameter of the PtPb NPs was 9.5 nm, and they exhibited a large particle-size distribution. In particular, the PtPb NPs are different sizes within the observation area even when the images were obtained from a single sample, as shown in Fig. S2. However, the Pt NPs (average diameter: 5.4 nm) were well dispersed on the WO_3 surface (the TEM images of the Pt NPs/WO_3 prepared through chemical and photodeposition are shown in Figs. S3 and S4). The HR-TEM image (C) of the interface between the PtPb and WO_3 phases shows clear lattice fringes, indicating that the PtPb NPs have atomically ordered structures on the WO_3 surface. Furthermore, the *d*-value is clearly different from that of WO_3. The interval of the lattice fringe (0.223 nm) on the PtPb phase is consistent with the *d*-value for the {110} planes of the ordered PtPb intermetallic phase (d = 0.213 nm, ICDD PDF File # 06-0374) but is not consistent with any *d*-values for Pt phases (fcc structure). The fast Fourier-transformation (FFT) pattern (Fig. S5) demonstrates that the atoms in the PtPb NPs are, as expected based on the *p*XRD data, arranged in a NiAs-type structure. The compositional maps (Fig. 2) based on the STEM images reveal that the Pt and Pb are uniformly distributed in the PtPb NPs. STEM-energy dispersive spectroscopy (EDS) maps in Fig. 2 demonstrate that the average molar ratios of Pt to Pb for the PtPb NPs (Pt:Pb = 56.2:43.8) were consistent with the desired values for PtPb (Pt:Pb = 1:1). Inductively coupled plasma-mass spectroscopy (ICP-MS) showed that the average molar ratio of Pt to Pb for the PtPb NPs on WO_3 was Pt:Pb = 49.8:50.2 for the as-prepared and annealed samples. The

*p*XRD and TEM/STEM data clearly indicate that an ordered intermetallic PtPb phase can be formed on a WO_3 surface through a one-pot process.

Fig. 3 shows the diffuse reflectance UV-Vis absorption spectra for the Pt NPs/WO_3 prepared from the Pt precursor on a WO_3 support when using $NaBH_4$ as the reducing agent. To evaluate the influence of the reducing agent on the support after the Pt ions were reduced in anhydrous methanol containing dispersed WO_3, UV-Vis spectra (Supplement information for the UV-Vis absorption spectroscopy procedure) were collected, as shown in Fig. 3A. Non-treated, pure WO_3 (a) exhibits an apparent absorption edge at 465 nm, as reported previously [16]. The as-prepared Pt NPs/WO_3 catalysts exhibit a visible absorption above 450 nm due to the reduction of the W^{6+} to W^{5+} or W^{4+}; the reducing agent reduced the Pt precursor in anhydrous methanol containing dispersed WO_3. A significant change in the visible absorption of the Pt NPs/WO_3 is induced through a heat treatment in air at 100 ºC over 1 h. Afterwards, the absorption band exhibited no obvious change compared to the pure WO_3, indicating that the oxidation state on the Pt NPs/WO_3 photocatalyst sample was restored to its original state. The XPS results obtained with the as-prepared and annealed Pt NPs/WO_3 also support our hypothesis regarding the change in the oxidation state of the W ions (Supplement information for the XPS procedure). The XPS spectra showing the W 4*f* region of (a) non-treated WO_3, (b) as-prepared Pt NPs/WO_3 and (c) annealed (100 ºC) Pt NPs/WO_3 are shown in Fig. 3B. All of the binding energies in Fig. 3B are assigned based on the literature values for WO_3 [17–19]. The XPS spectra were curve-fitted, and each curve was assigned to the corresponding oxidation state in the W 4*f* level. A doublet was used to fit the W 4*f* level, as observed in Fig. 3B-(a). The peak for W $4f_{7/2}$ can be observed at 35.4 eV and is generated by the photoelectrons emitted from W^{+6} species (WO_3). The spectrum (b) recorded with the as-prepared Pt NPs/WO_3 can be

assigned two doublets: the peak (W $4f_{7/2}$) of the first doublet is located at 35.4 eV and is generated by photoelectrons emitted from W^{+6} species; the peak (W $4f_{7/2}$) for the second doublet is located at 34.4 eV and can be attributed to the photoelectrons emitted from tungsten atoms near the oxygen vacancies formed by the reduction reactions when the oxidation state of W is below +6. As observed in (c), the second doublet was removed after treating the Pt NPs/WO_3 at 100 ºC, reforming the W^{6+}. For the PtPb NPs/WO_3, a clear absorbance change could be observed between non-treated WO_3 and as-prepared PtPb NPs/WO_3 (Fig. S6-A), but no drastic changes were observed in the oxidation state of WO_3 based on the XPS spectra (Fig. S6-B). The annealing process (in air at 100 ºC for 1 h) was applied to the as-prepared PtPb NPs/WO_3 samples to return the optical properties of the WO_3 in PtPb NPs/WO_3 to that of the untreated WO_3 supports. The UV-Vis absorption spectra of the annealed Pt NPs/WO_3 and annealed PtPb NPs/WO_3 are overlaid in Fig. S7 to compare their optical absorption properties. The Pt NPs/WO_3 exhibit a higher visible absorption than the PtPb NPs/WO_3.

The photocatalytic activities of the photodeposited Pt NPs/WO_3, chemically deposited Pt NPs/WO_3 and annealed PtPb NPs/WO_3 photocatalysts were examined during a photocatalytic decomposition of AcOH in aerated aqueous suspensions (Supplementary information contains the procedure used to evaluate the decomposition rate of the AcOH). Fig. 4(A) plots the CO_2 generated during the liquid-phase decomposition of AcOH over the Pt NPs- and PtPb NPs-loaded WO_3. The rates of CO_2 generation over the Pt NPs/WO_3 and PtPb NPs/WO_3 photocatalysts were estimated using the slope of the CO_2 formation *vs.* time plot from 0-100 min. The CO_2 generation rate over the PtPb NPs/WO_3 (115.3 $\mu mol \cdot mg_{\text{-Pt}}^{-1} \cdot h^{-1}$) was higher than that of the photodeposited- (56.33 $\mu mol \cdot mg_{\text{-Pt}}^{-1} \cdot h^{-1}$) and chemically deposited (50.24 $\mu mol \cdot mg_{\text{-Pt}}^{-1} \cdot h^{-1}$) Pt NPs/$WO_3$. The low activity of the annealed-chemically deposited Pt NPs/WO_3

versus the photodeposited Pt NPs/WO_3 might be attributed to the reduced tungsten ions in the WO_3 in the annealed-chemically deposited Pt NPs/WO_3. However, the XPS data in Fig. 3B-c do not show any XPS peaks attributed to reduced tungsten ions (W^{5+} or W^{4+}) after annealing. Therefore, the contradictory data from the activity test and XPS measurements should be examine. Although the low activity of the annealed-chemically deposited Pt NPs/WO_3 is attributed to a small change in the oxidation state of the tungsten ions that cannot be detected through XPS, we propose that the differences in the deposition sites of the Pt NPs on the WO_3 of the annealed-chemically deposited Pt NPs/WO_3 and photodeposited Pt NPs/WO_3 samples should also be examined. In the annealed-chemically deposited Pt NPs/WO_3 the Pt NPs were randomly deposited on the WO_3 surfaces. On the surfaces of the photodeposited Pt NPs/WO_3 sample, however, the Pt NPs were site-selectively deposited on the WO_3. Because the Pt NPs were formed by reductive deposition with photoexcited electrons, the Pt NPs were deposited on the site (reduction site) where the photoexcited electrons appear on the surfaces of the WO_3. The co-catalysts deposited on the reduction site actively catalyze the reduction reaction under visible light. Fig. 4(B) shows the AcH decomposition and CO_2 generation profiles over WO_3 that was annealed after exposure to a reducing agent, photodeposited- and chemically deposited Pt NPs/WO_3, and annealed PtPb NPs/WO_3 photocatalysts under visible light irradiation ($\lambda > 420$ nm) (Supplementary information details the procedure used to evaluate the decomposition rate of AcH). With visible light irradiation, the amounts of AcH in the gas phase over the Pt NPs/WO_3 and PtPb NPs/WO_3 decreased rapidly when the CO_2 generation increased versus WO_3. The complete decomposition of AcH is proven by the molar yield of CO_2 (ca. 530 ppm), which is twice that of the molar amount of AcH injected (ca. 280 ppm). The Pt NPs/WO_3 and PtPb NPs/WO_3 photocatalysts completely decomposed AcH to form CO_2 over different reaction times.

In contrast, WO_3 could not decompose AcH completely because the catalyst was deactivated by the products that accumulated on its surface [20]. Of the examined samples, PtPb NPs/WO_3 perform the best by completely decomposing AcH to CO_2 within 120 min.

Conclusion

Samples of WO_3 loaded with Pt and PtPb NPs were used to photocatalyze the decomposition of organic compounds in the liquid and gas phases with visible light irradiation ($\lambda > 420$ nm). PtPb NPs/WO_3 exhibit a higher photocatalytic activity than the conventional Pt NPs/WO_3 and the pure WO_3. This enhanced photocatalytic activity might be attributed to the efficient multi-electron ORR and the oxidative decomposition of organic compounds, which induces charge separations in the PtPb. The particles of the ordered PtPb intermetallic NPs on WO_3 are much larger than the Pt NPs on WO_3; the Pt NPs on WO_3 have much larger surface areas exposed to the AcOH solution and to the gas phase containing AcH than the PtPb NPs fixed on WO_3. Although the surface area of the PtPb NPs is smaller than that of the reported catalysts utilized in this work, the Pt NPs/WO_3 exhibit a higher visible absorption than the PtPb NPs/WO_3; PtPb showed enhanced photocatalytic activity relative to the Pt NPs/WO_3. Therefore, the surfaces of the ordered intermetallic PtPb NPs are more efficient as co-catalysts on WO_3. Our strategy for preparing PtPb NPs on WO_3 was successful, and the results demonstrate highly efficient visible light-induced photocatalytic systems using ordered intermetallic NP co-catalysts.

Acknowledgements

We thank Dr. Akihiro Yoshida and Prof. Shuichi Naito of Kanagawa University for help measuring photocatalytic activity. This work was financially supported by the

Strategic Research Base Development Program for Private Universities of the Ministry of Education, Culture, Sports, Science and Technology of Japan.

Reference

[1] A. Fujishima, T.N. Rao, D.A. Tryk, J Photoch Photobio C 1(2000) 1-21.

[2] K. Maeda, K. Domen, J. Phys. Chem. Lett. 1 (2010) 2655-2661.

[3] K. Mori, H. Yamashita, M. Anpo, RSC Adv. 2 (2012) 3165-3172.

[4] M.G. Walter, E.L. Warren, J.R. McKone, S.W. Boettcher,Q. Mi, E.A. Santori, N.S. Lewis, Chem. Rev. 110 (2010) 6446-6473.

[5] K. Maeda, M. Higashi, D. Lu, R. Abe, K. Domen, J. Am. Chem. Soc. 132 (2010) 5858-5868.

[6] G. R. Bamwenda, H. Arakawa, Appl. Catal. A 210 (2001) 181-191.

[7] R. Abe, H. Takami,N. Murakami, B. Ohtani, J. Am. Chem. Soc. 130 (2008) 7780-7781.

[8] E. Casado-Rivera, Z. Gál, A.C.D. Angelo, C. Lind, F.J. DiSalvo, H.D. Abruña, ChemPhysChem 4 (2003) 193-199.

[9] E.D. Casado-Rivera, J. Volpe, L. Alden, C. Lind, C. Downie, T. Vázquez-Alvarez, A.C.D. Angelo, F.J. DiSalvo, H.D. Abruña, J. Am. Chem. Soc. 126 (2004) 4043-4049.

[10] Y. Kang, L. Qi, M. Li, R.E. Diaz, D. Su, R.R. Adzic, E. Stach, J. Li, C.B. Murray, ACS Nano 6 (2012) 2818-2825.

[11] L.D. Shao, W. Zhang, M. Ambruster, D. Teschner, F. Girgsdies, B.S. Zhang, O. Timpe, M. Friedrich, R. Schlogl, D.S. Su, Angew. Chem., Int. Ed. 50 (2011) 10231-10235.

[12] A.C. Chen, P.H.-Hindle, Chem. Rev. 110 (2010) 3767-3804.

[13] H. Abe, F. Matsumoto, L.R. Alden, S. C. Warren, H. D. Abruna, F.J. DiSalvo, J. Am. Chem. Soc. 130(2008) 5452-5458.

[14] F. Matsumoto, C. Roychowdhury, F.J. DiSalvo and H.D. Abruña, J. Electrochem. Soc. 155 (2008) B148-B154.

[15] T. Gunji, G. Saravanan, T. Tanabe, T. Tsuda, M. Miyauchi, G. Kobayashi, H. Abe, F. Matsumoto, Catal. Sci. Technol. 4(2014) 1436-1445.

[16] D. Tsukamoto, M. Ikeda, Y. Shiraishi, T. Hara, N. Ichikuni, S. Tanaka, T. Hirai, Chem. Eur. J. 17 (2011) 9816-9824.

[17] W. Li, J. Li, X. Wang, Q. Chen, Applied Surface Science 263 (2001) 157-162.

[18] A. Mozalev, V. Khatko, C. Bittencourt, A.W. Hassel, G. Gorokh, E. Llobet, X. Correig, Chemistry of Materials 20 (2008) 6482–6493.

[19] W. Li, Z. Fu, Applied Surface Science 256 (2010) 2447–2452.

[20] T. Arai, M. Yanagida, Y. Konishi, Y. Iwasaki, H. Sugihara, K. Sayama, J. Phys. Chem. C 111(2007) 7574-7577.

Figure captions

Fig. 1 (A) *p*XRD diffractograms of the WO_3 (a), Pt NPs/WO_3 (b) and PtPb NPs/WO_3 (c) (for b and c, 5 wt% Pt on WO_3). (B) TEM image of the annealed PtPb NPs/WO_3 photocatalyst (1.0 wt% PtPb on WO_3) and (C) a high-resolution (HR)-TEM image of the interface between the PtPb and WO_3 phases. The marks (* and #) in (A) correspond to the peaks for Pt and PtPb, respectively.

Fig. 2 Scanning transmission electron microscopy (STEM) image of the annealed PtPb NPs/WO_3 (PtPb loading weight on WO_3: 1.0 wt%) and the corresponding compositional mapping images.

Fig. 3 (A) Diffuse reflectance UV-Vis absorption spectra for the (a) non-treated WO_3, (b) as-prepared Pt NPs/WO_3 and (c) annealed (100º C) Pt NPs/WO_3 (for b and c, 1.0 wt% Pt on WO_3). (B) XPS spectra (red lines) and fitted curves (blue lines) in the W 4*f* region for the (a) non-treated WO_3, (b) as-prepared Pt NPs/WO_3 and (c) annealed (100º C) Pt NPs/WO_3.

Fig. 4 (A) The time courses of the CO_2 evolution during the decomposition of AcOH over the chemically deposited Pt NPs/WO_3 (solid circle, 1 wt % Pt), photodeposited Pt NPs/WO_3 (solid triangle, 1 wt % Pt) and annealed PtPb NPs/WO_3 (1 wt% PtPb, solid square) photocatalysts suspended in aqueous AcOH in the presence of O_2 with visible light irradiation ($\lambda > 420$ nm). (B) The time trials for the decomposition of AcH (open symbol) and the evolution of CO_2 (solid symbol) in the presence of O_2 over WO_3 (cross), Pt/WO_3 (triangle, Pt was deposited by photo deposition, 0.1 wt % Pt), Pt NPs/WO_3 (circle, Pt was deposited by chemical deposition, 0.1 wt % Pt) and annealed PtPb NPs/WO_3 (square, 0.1 wt% PtPb) photocatalysts with visible light irradiation ($\lambda >$ 420 nm).

Figures

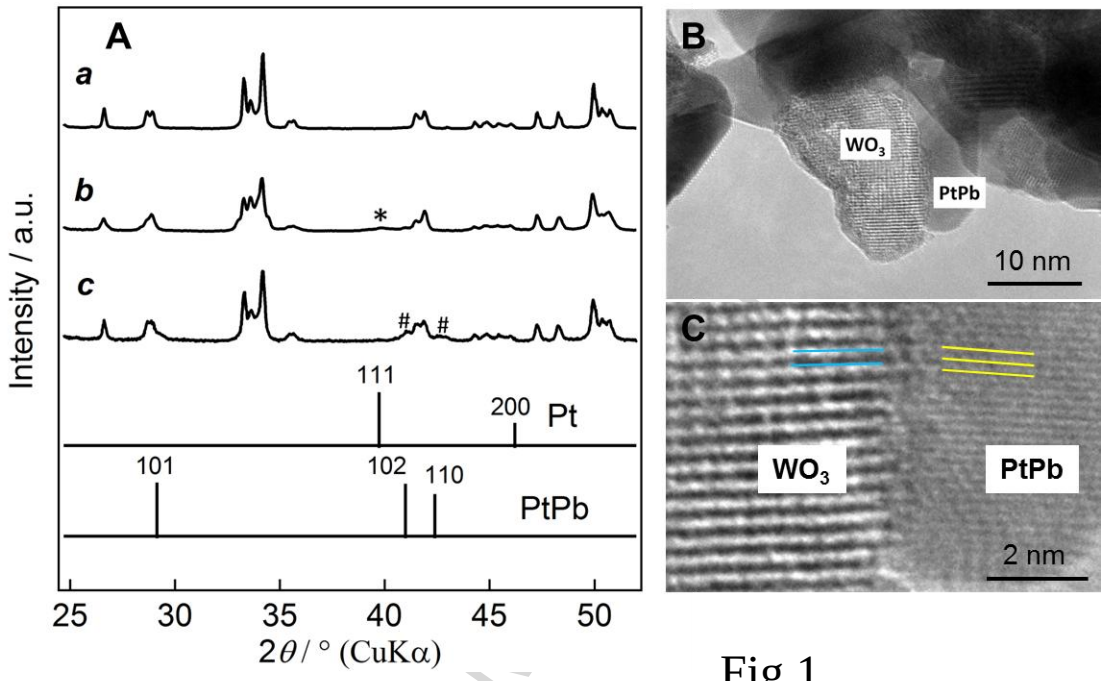

Fig.1

T. Gunji *et al.*

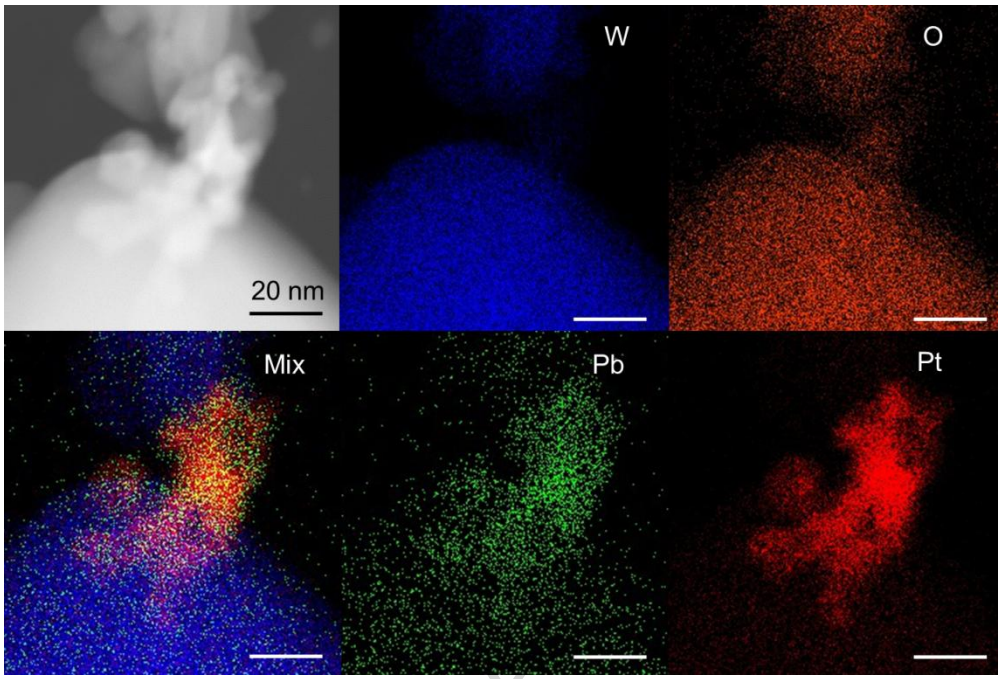

Fig. 2

T. Gunji *et al.*

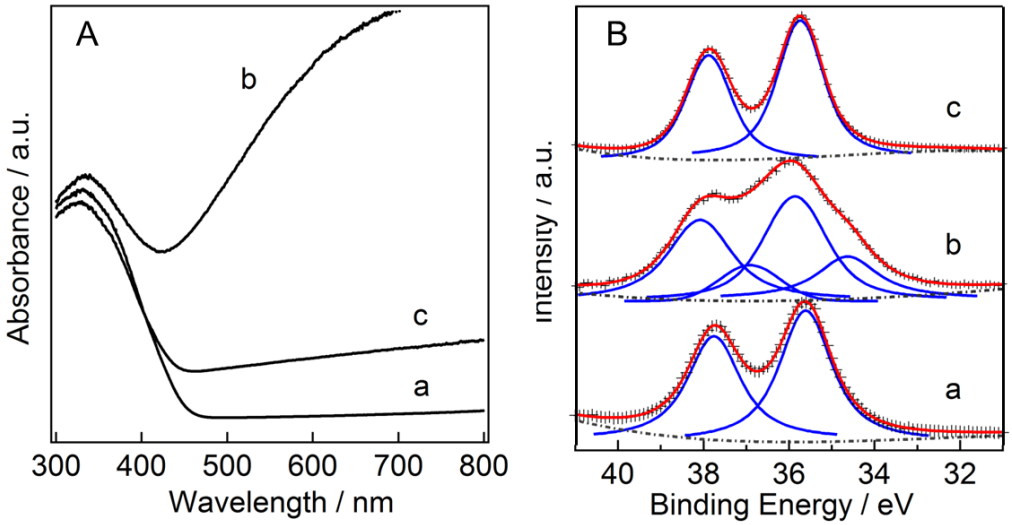

Fig. 3

T. Gunji *et al.*

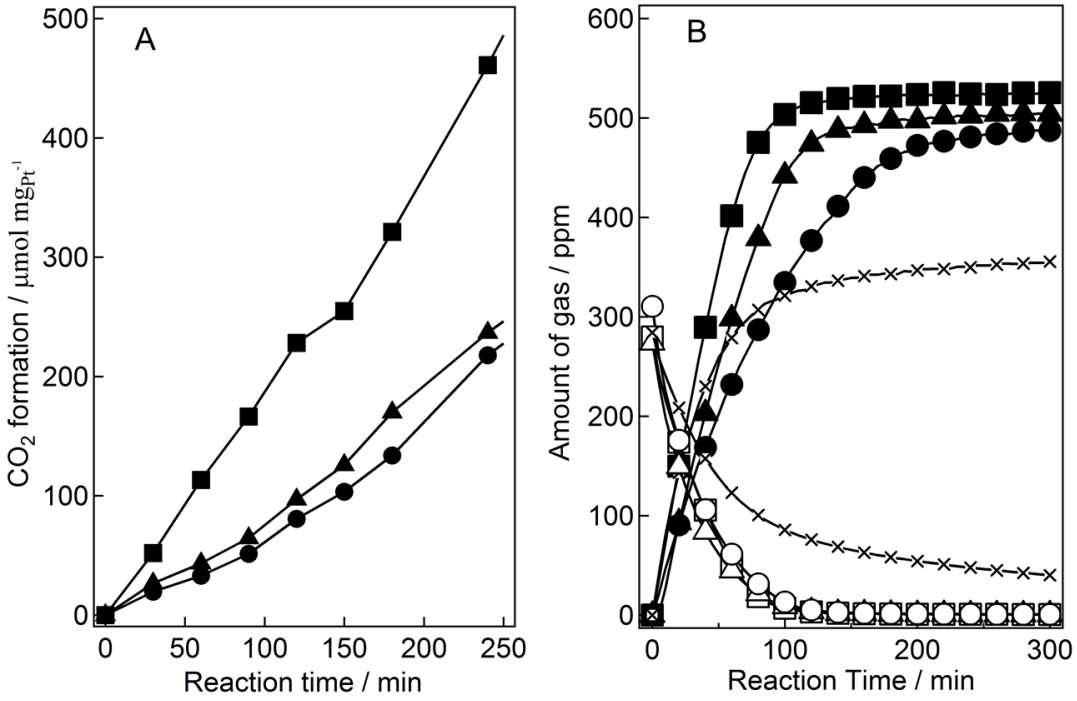

Fig. 4

T. Gunji *et al.*

Graphical Abstract

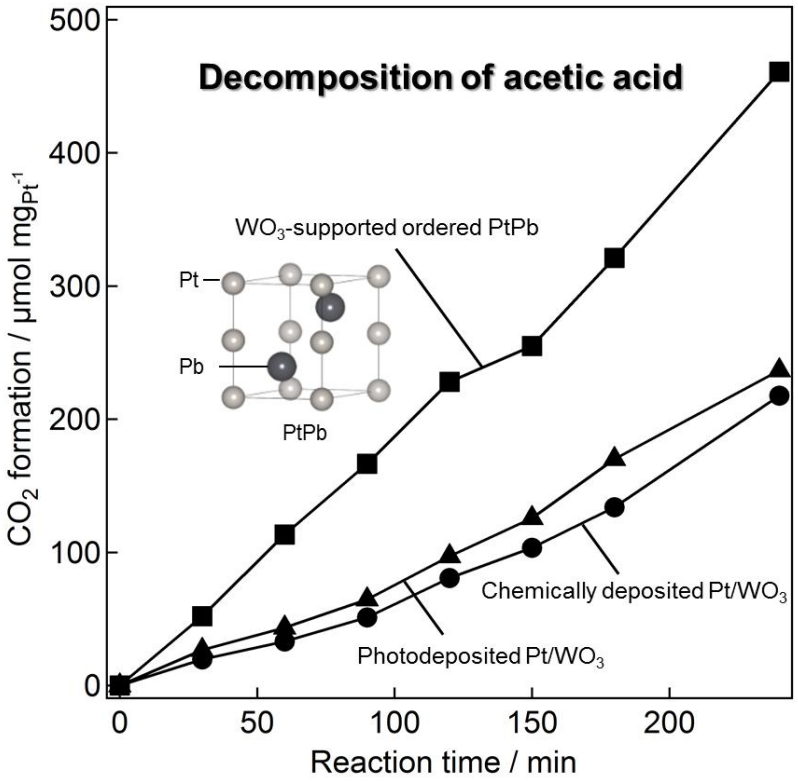

Highlights

- The WO_3 supported PtPb catalysts was synthesized
- The formation of $PtPb/WO_3$ catalysts were characterized with TEM and XPS
- The photocatalytic activities of the $PtPb/WO_3$ were investigated
- $PtPb/WO_3$ showed higher catalytic activity for decomposition of AcOH and AcH than Pt/WO_3